

***Ab initio* study of ferromagnetic single-wall nickel nanotubes**

Takahiro Shimada,\* Yoshiyuki Ishii, and Takayuki Kitamura

*Department of Mechanical Engineering and Science, Kyoto University, Sakyo-ku, Kyoto 606-8501, Japan*

(Received 8 September 2011; published 27 October 2011)

We performed *ab initio* spin-density functional theory calculations of the magnetic and electronic properties of ferromagnetic single-wall nickel nanotubes with various chiralities. A (6,3) nanotube was found to have an energetically favorable “magic” structure and consequently it is expected to be observed experimentally for both free-standing and tip-suspended conditions, whereas a (5,3) nanotube is expected to be observed only in the free-standing case. The (6,3) and (5,3) nanotubes, respectively, exhibit enhanced magnetic moments of  $0.864 \mu_B$  and  $0.774 \mu_B$  relative to  $0.635 \mu_B$  in Ni bulk, because of their low coordination numbers. The dependence of the magnetic moment on the chirality is predominated by the minority-spin  $d_{xy}$  and  $d_{zx}$  states in which the out-of-plane  $d$  orbitals interact strongly with each other due to the nanotube curvature.

DOI: [10.1103/PhysRevB.84.165452](https://doi.org/10.1103/PhysRevB.84.165452)

PACS number(s): 75.75.-c, 61.46.Fg, 31.15.A-

**I. INTRODUCTION**

In recent years, nanotubes and nanowires have attracted considerable attention as one-dimensional nanostructures because their electronic and mechanical properties<sup>1-4</sup> differ greatly from those of bulk materials and they are very promising for use in industrial applications such as in the fabrication of electronic devices. As technological progress strongly demands miniaturization of device components, various fabrication techniques have been developed to synthesize very thin metallic wires that are several nanometers in diameter.<sup>5-10</sup> In particular, Takayanagi and co-workers<sup>5,6</sup> successfully fabricated a tip-suspended gold nanowire with a diameter less than 2 nm in an ultrahigh-vacuum transmission electron microscopy (UHV-TEM). Interestingly, this very thin nanowire exhibits a helical multishell structure that has a specific “magic” size, as predicted theoretically.<sup>11</sup> Furthermore, they have also synthesized a single-wall helical gold nanotube with a smaller diameter of 0.4 nm in a UHV-TEM.<sup>7</sup> Such single-wall helical nanotubes and helical multishell nanowires have been intensively fabricated experimentally and investigated theoretically not just for Au<sup>1,5-7,11-16</sup> but also for various metals (e.g., Ag, Pt, Na, Rh, Zr, Ti, Pb, and ferromagnetic Ni).<sup>2,3,17-24</sup> These studies have reported that the nanotubes and nanowires possess distinct mechanical and electronic properties originating from their helical shell structure, including superplasticity,<sup>3</sup> quantum ballistic conductance,<sup>4</sup> and helical conduction channels (which potentially could be used to fabricate nanosolenoid).<sup>1,2</sup> However, to the best of our knowledge, there has been no detailed study on the magnetism of helical nickel nanotubes or nanowires.

Nickel is a typical face-centered cubic (fcc) metal that exhibits ferromagnetism. Single-wall nanotubes of an fcc metal can be made by rolling a two-dimensional triangular lattice of a (111) monolayer in a specific chiral direction. Since nickel nanotubes have extremely low coordination numbers, the reduced interaction between neighboring atoms is expected to give rise to distinct magnetic and electronic properties from that of the counterpart bulk. In addition, the magnetism is expected to be strongly dependent on the tube chirality, because the nanotubes with different chiralities have different electronic states.<sup>1,2,12,18</sup> Thus, studying ferromagnetic nickel

nanotubes should lead to a deeper understanding of magnetism in nanostructures.

Theoretical studies based on *ab initio* (first-principles) density functional theory (DFT) calculations have successfully provided comprehensive insight into both the stability of metallic nanotubes<sup>1,2,11,18</sup> and the magnetic properties of various nanostructures.<sup>25-28</sup> In this study, we perform DFT calculations to investigate the magnetism as well as structural, energetic, and electronic properties in nickel single-wall nanotubes. The remainder of the paper is structured as follows. Section II describes the simulation procedure in detail. In Sec. III, the structural, energetic, magnetic, and electronic properties of the nickel single-wall nanotubes are presented by focusing on their helical shell structure. Finally, Sec. IV summarizes the results of this study.

**II. COMPUTATIONAL DETAILS****A. Simulation method**

*Ab initio* (first-principles) spin-density-functional theory calculations are performed using the Vienna *Ab-initio* Simulation Package (VASP) code.<sup>29,30</sup> The electronic wave functions are expanded in plane waves up to a cutoff energy of 350 eV. The electron-ion interaction is described by the projector-augmented-wave (PAW) potential<sup>31,32</sup> that explicitly includes the Ni 3*d* and 4*s* electrons in the valence states. The PAW approach is essential for obtaining an accurate description of magnetism in transition-metal nanostructures<sup>33</sup> because it realizes the computational efficiency of the pseudopotential method and the accuracy of all-electron method, which do not suffer from problems regarding the linearization of the core-valence exchange interaction. To evaluate the exchange-correlation energy, we employ the generalized gradient approximation (GGA) of the Perdew-Burke-Ernzerhof (PBE) functional.<sup>34</sup>

**B. Simulation models and procedure**

Figure 1 shows the chiral vector  $C_v$  of the two-dimensional triangular lattice of a nickel (111) monolayer. The chiral vector uniquely defines the circumferential structure of Ni nanotubes,

$$C_v = m\mathbf{a}_1 + n\mathbf{a}_2 \equiv (m, n), \quad (1)$$

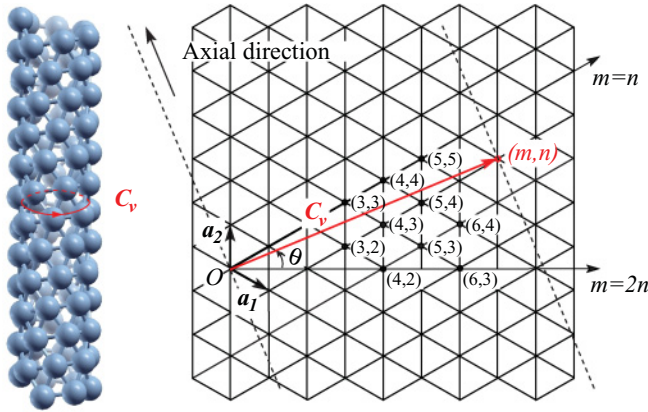


FIG. 1. (Color online) Schematic illustration depicting the chiral vector  $C_v$  on the two-dimensional triangular lattice of the nickel (111) monolayer. The chiral vector is represented by  $C_v = m\mathbf{a}_1 + n\mathbf{a}_2$ , where  $\mathbf{a}_1$  and  $\mathbf{a}_2$  denote the primitive translation vectors. The chiral angle is denoted by  $\theta$ .

and it connects two crystallographically equivalent sites on the (111) monolayer. Here,  $\mathbf{a}_1$  and  $\mathbf{a}_2$  denote the primitive cell vectors of the (111) monolayer, and the chiral angle  $\theta$  is defined as the ascending angle from the horizontal line of  $m = 2n$ . Due to the symmetry of the triangular lattice, all possible configurations of the single-wall nanotubes can be represented by chiral vectors within the irreducible area enclosed by the two lines of symmetry,  $m = 2n$  and  $m = n$ , in which the chiral angle  $\theta$  ranges from  $0^\circ$  to  $30^\circ$ .<sup>2</sup>

Figure 2 shows simulation models of nickel nanotubes with different chiralities. In this study, we simulate (3,2) ~ (6,4) single-wall nanotubes (see also Fig. 1), because single-wall nanotubes with larger diameters are relatively unstable for a helical multishell or crystalline nanowire.<sup>20</sup> Table I lists the initial structural parameters of the nickel ( $m,n$ ) nanotubes. A diameter of ( $m,n$ ) nanotube,  $D$ , is given by

$$D = \frac{d}{\pi} \sqrt{m^2 + n^2 - mn}, \quad (2)$$

where  $d$  is the Ni-Ni bond length of the flat monolayer,  $d = 2.356 \text{ \AA}$ . The axial cell dimension  $L_z$  of each nanotube is taken to be the minimum length to ensure helical periodicity. Since three-dimensional periodic boundary conditions are applied, a vacuum thickness of  $l_v = 15 \text{ \AA}$  is introduced in both

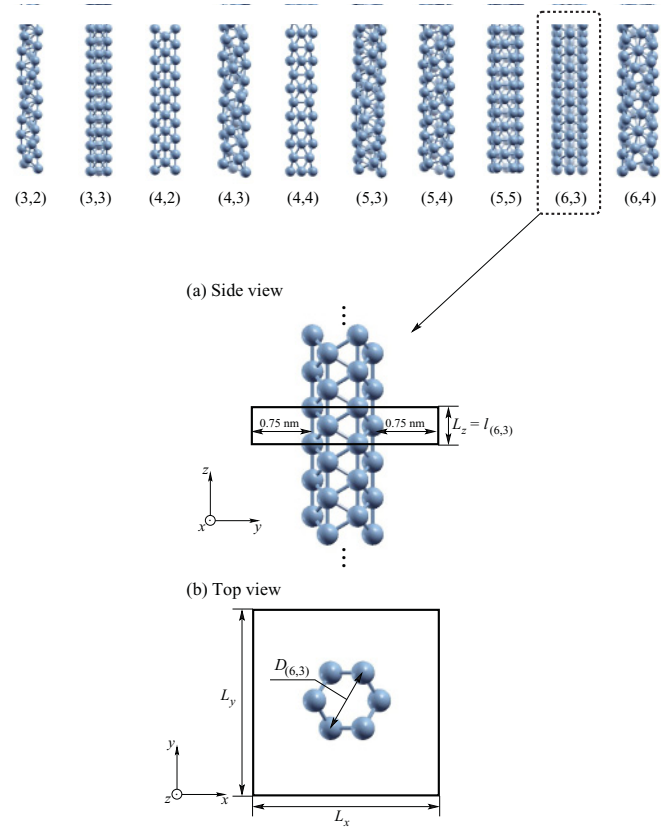


FIG. 2. (Color online) Simulation models of single-wall nickel nanotubes with different chiralities ( $m,n$ ). (a) Side view and (b) top view of the (6,3) nanotube. The black solid boxes represent the simulation cell.

the  $x$  and  $y$  directions to ensure that undesirable interactions between neighboring nanotubes are sufficiently canceled out. Thus, the simulation cell dimension in the  $x$  and  $y$  directions is set to  $D + l_v$ . The Brillouin zone (BZ) integrations are carried out using the Monkhorst-Pack  $k$ -point mesh<sup>35</sup> shown in Table I. The ferromagnetic (FM) phase is considered<sup>25</sup> for all the nanotubes.

To obtain an equilibrium nanotube structure, the atomic positions and the cell size in the axial  $z$  direction are fully relaxed using the conjugate gradient (CG) method until all the

TABLE I. Initial structural parameters of nickel nanotubes simulated in this study.

Chiral index	Chiral angle $\theta$ (degree)	Initial diameter $D$ ( $\text{\AA}$ )	Axial cell length $L_z$ ( $\text{\AA}$ )	Number of atoms $N$	Number of $k$ points $k_x \times k_y \times k_z$
(3,2)	10.9	1.98	10.81	14	$2 \times 2 \times 8$
(3,3)	30.0	2.25	4.08	6	$2 \times 2 \times 16$
(4,2)	0.0	2.60	2.36	4	$2 \times 2 \times 24$
(4,3)	16.1	2.71	14.78	26	$2 \times 2 \times 6$
(4,4)	30.0	3.00	4.08	8	$2 \times 2 \times 16$
(5,3)	6.6	3.27	17.82	38	$2 \times 2 \times 6$
(5,4)	19.1	3.44	6.24	14	$2 \times 2 \times 10$
(5,5)	30.0	3.75	4.08	10	$2 \times 2 \times 16$
(6,3)	0.0	3.90	2.36	6	$2 \times 2 \times 20$
(6,4)	10.9	3.97	10.81	28	$2 \times 2 \times 8$

TABLE II. Structural and energetic properties of the single-wall nickel nanotubes. For comparison, those of the atomic sheet of nickel monolayer are also shown.

Ni nanotube	Diameter $D$ (Å)	Axial length $L_z$ (Å)	Averaged bond length $d_{ave}$ (Å)	Total energy per atom $E_{tot}/N$ (eV/atom)	Binding energy $E_B$ (eV/atom)	String tension $f$ (eV/Å)
(3,2)	2.47	10.59	2.378	-4.0407	3.304	2.03
(3,3)	2.69	3.99	2.379	-4.1877	3.451	2.16
(4,2)	2.90	2.37	2.370	-4.2605	3.524	2.22
(4,3)	3.00	14.76	2.371	-4.2622	3.526	2.31
(4,4)	3.25	4.09	2.372	-4.2918	3.555	2.51
(5,3)	3.47	17.99	2.365	-4.3308	3.594	2.63
(5,4)	3.64	6.30	2.365	-4.3204	3.584	2.77
(5,5)	3.95	4.10	2.364	-4.3348	3.598	3.06
(6,3)	4.05	2.37	2.361	-4.3798	3.643	3.02
(6,4)	4.13	10.85	2.360	-4.3752	3.639	3.10
Sheet	—	—	2.356	-4.3994	3.663	—

Hellmann-Feynman forces and the stress component  $\sigma_{zz}$  are less than  $2.5 \times 10^{-3}$  eV/Å and  $1.0 \times 10^{-2}$  GPa, respectively.

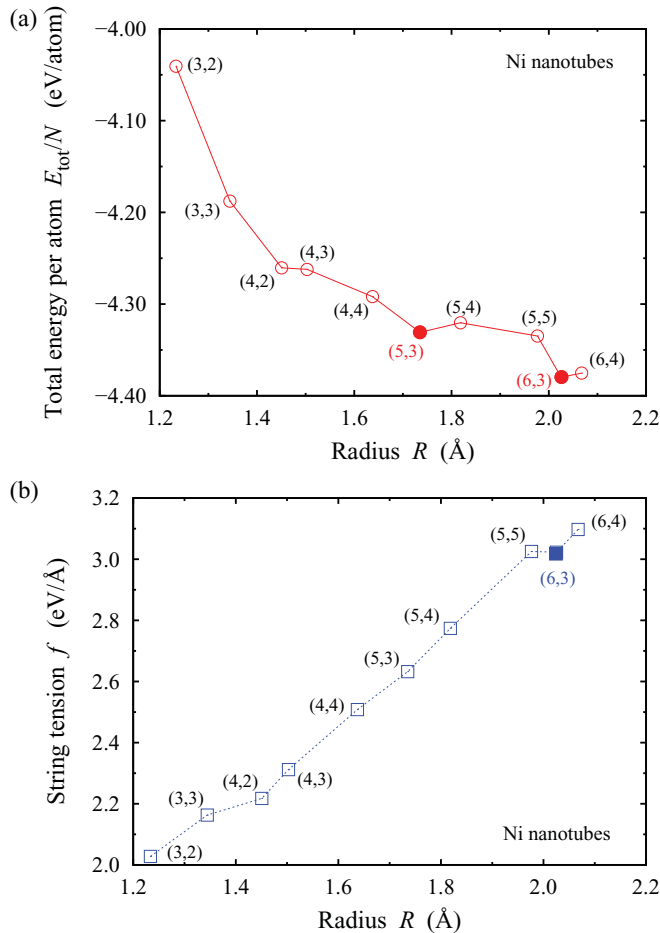


FIG. 3. (Color online) (a) Total energy per atom  $E_{tot}/N$  as a function of nanotube radius  $R$  for the nickel nanotubes. (b) String tension  $f$  as a function of nanotube radius  $R$ . The solid symbols indicate the local minimum along each curve.

### III. RESULTS AND DISCUSSION

#### A. Structural and energetic properties of single-wall nickel nanotubes

Table II summarizes the structural and energetic properties of the relaxed nickel nanotubes. Those of a flat nickel monolayer (sheet) are also shown for comparison. The optimized tube diameter  $D$  increases from the initial tube diameter that is simply produced by rolling the nickel monolayer (see also Table I). This increase is remarkable in thin nanotubes because such nanotubes deform to relax their high strain energies due to their large curvature. Consequently, thinner nanotubes have a longer average bond length  $d_{ave}$ , whereas the average bond lengths of the (6,3) and (6,4) nanotubes, which have low curvatures, are slightly longer than that of the flat sheet.

The total energy per atom  $E_{tot}/N$  decreases with increasing tube radius. The binding energy (a related quantity)  $E_B = E_{atom} - E_{tot}/N$ , where  $E_{atom}$  is the total energy of an isolated nickel atom, is positive (exothermic) for all the nanotubes. This indicates a stable structure corresponding to a local minimum on the Born-Oppenheimer surface.<sup>1</sup> The  $E_B$ - $R$  relationship suggests that the nanotubes with larger  $D$  are generally more stable. However, the trend is not always monotonic. Figure 3(a) shows a plot of the total energy per atom  $E_{tot}/N$  as a function of the nanotube radius  $R = D/2$  for the nickel nanotubes. There are local minima at the (5,3) and (6,3) nanotubes. As discussed by Elizondo and Mintmire,<sup>2</sup> local energy minima correspond to a long-lived metastable state of nanotubes in a free-standing condition. In fact, an experimentally synthesized silver nanotube<sup>17</sup> corresponds to the theoretically predicted local minimum structure of the (4,2) nanotube.<sup>2</sup>

We calculated the string tension  $f$  of a nanotube, which is defined by considering the positive work required to draw a tube out of the bulk material. It is given by  $f = (F - \mu N)/L_z$ .<sup>11</sup> Here,  $\mu$  is the chemical potential of bulk nickel and  $F$  is the free energy of a nanotube, which equals the total energy ( $F = E_{tot}$ ) at zero temperature ( $T = 0$  K). As discussed in a previous study,<sup>11</sup> the string tension  $f$  is an important parameter for describing the stability of a nanotube in a tip-suspended condition which is often experimentally the case. The string tension  $f$  as a function of the radius

$R$  is shown in Fig. 3(b). The string tension increases with increasing tube radius, but not monotonically around the (6,3) nanotube. The (6,3) nanotube has a lower string tension than its immediate neighboring structures, which indicates that the (6,3) nanotube is a long-lived “magic” structure of nickel nanotubes. In fact, a gold (5,3) nanotube that was predicted to be stable based on string tension consideration<sup>11</sup> was experimentally observed in a tip-suspended condition during the thinning process of gold nanowires.<sup>7</sup>

Thus, our DFT calculations predict that the Ni(6,3) nanotube will be energetically stable and should be observed experimentally in both the free-standing and tip-suspended conditions, whereas the Ni(5,3) nanotube is expected to be observed only in the free-standing case.

### B. Magnetic and electronic properties of stable nickel nanotubes

Table III shows the magnetic moments  $M$  of stable (6,3) and (5,3) nickel nanotubes. For comparison, those of the flat monolayer and nickel bulk are also shown. The nanotubes and monolayer exhibit higher magnetic moments than the bulk because the nanotubes and monolayer possess a lower coordination number of 6 with respect to that of 12 in the bulk, which narrows minority-spin bands and reduces the number of minority-spin electrons.<sup>28</sup> The (6,3) nanotube has approximately the same magnetic moment as the monolayer, whereas the (5,3) nanotube possesses a magnetic moment that is lower by  $0.12 \mu_B$ , despite having the same coordination number. This indicates that the magnetism depends sensitively on the chiral nanotubular structure.

For a more detailed discussion, we calculated the difference in the number of  $d$  electrons (which predominate the magnetism of nickel) between the monolayer and the (6,3) or (5,3) nanotubes (see Fig. 4). A remarkable difference is observed in the minority-spin state in both the nanotubes, whereas the majority-spin state is almost insensitive. There is also a strong angular dependence on each  $d$  component in the minority-spin state: The number of electrons increases for the  $d_{xy}$  and  $d_{zx}$  states, remarkably in the (5,3) nanotube, while it decreases for the other  $d_{yz}$ ,  $d_{z^2}$ , and  $d_{x^2-y^2}$  states. Thus, the relatively small magnetic moment of the (5,3) nanotube originates from the considerable increase in the minority-spin  $d_{xy}$  and  $d_{zx}$  states. Note that a similar increase is also found in the (6,3) nanotube, but is somewhat moderate. Since, in this case, the increase is comparable to the reduction in the  $d_{yz}$ ,  $d_{z^2}$ , and  $d_{x^2-y^2}$  states, the (6,3) nanotube exhibits almost the same magnetic moment as the monolayer.

Figures 5(a)–5(c) show the total and partial  $d$  spin-polarized electronic local density of states (DOS) of the nickel (111) monolayer, and the (6,3) and (5,3) nanotubes, respectively. The majority-spin state distributes below the Fermi level  $E_F$ , and is fully occupied in both the monolayer and the nanotubes.

TABLE III. Magnetic moments  $M$  of the stable (6,3) and (5,3) nickel nanotubes. For comparison, those of the flat monolayer and nickel bulk are also shown.

	(6,3)	(5,3)	Sheet	Bulk
$M$ ( $\mu_B$ )	0.864	0.774	0.894	0.635

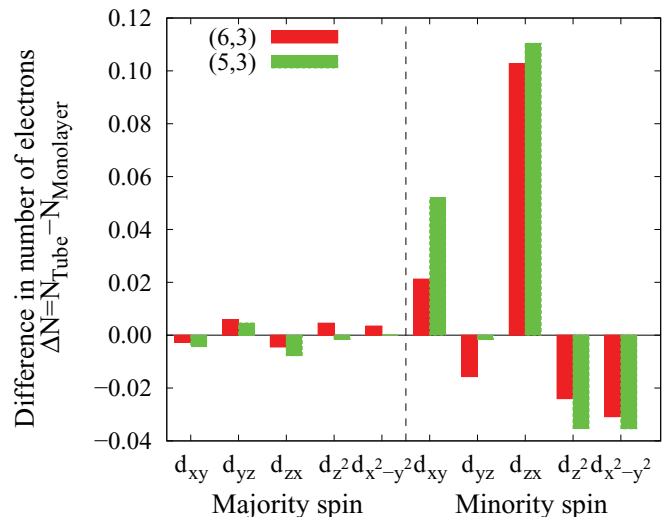


FIG. 4. (Color online) Difference in number of majority-spin and minority-spin electrons in each  $d$  component between the monolayer and the (6,3) or (5,3) nanotube,  $\Delta N = N_{\text{Tube}} - N_{\text{Monolayer}}$ .

This reasonably explains why these structures have the same number of majority spins. In contrast, the minority-spin state is partially occupied. This suggests that the magnetic moment is sensitively affected by the difference in the minority-spin DOS between the monolayer and the nanotubes, as discussed below. In the monolayer, three  $d_{yz}$ ,  $d_{z^2}$ , and  $d_{x^2-y^2}$  minority-spin states are widely distributed between  $-3$  eV and  $0.8$  eV (the bandwidth is  $3.8$  eV). Because these three  $d$  states mainly possess in-plane orbitals [see the schematic illustration of topology of  $d$  orbitals on the monolayer as shown in Fig. 5(d)], each  $d$  orbital directly interacts with the  $d$  orbitals of its neighboring atoms and forms strong  $dd\sigma$  bonds. Thus, the large width of these subbands results from the formation of a  $dd\sigma$  bond. On the other hand, other two  $d_{xy}$  and  $d_{zx}$  states have a narrower bandwidth of  $2.3$  eV relatively localized with the range from  $-1.8$  to  $0.5$  eV. These two  $d$  orbitals interact indirectly with each other because of their out-of-plane topologies [see also Fig. 5(d)] and form a weaker  $dd\pi$  bond than the  $dd\sigma$  bond. This weaker interaction produces the narrower bandwidth. For the case of the nanotubes, there is a distinct difference in the minority-spin DOS: The  $d_{xy}$  and  $d_{zx}$  states are widely distributed about  $-2.5 \sim 0.8$  eV (width of  $3.3$  eV). Compared to the monolayer, these two  $d$  states are distributed in lower energy levels in the nanotubes, which increases the number of minority-spin electrons (see Fig. 4). This can be explained by considering the nanotubular and  $d$ -orbital geometries: The interactions of  $d_{xy}$  and  $d_{zx}$  orbitals are strengthened by the tube curvature due to the out-of-plane topology, as schematically shown in Fig. 6 for the  $d_{xy}$  orbital. The interaction should be stronger in the (5,3) nanotube than in the (6,3) nanotube because the former has a larger curvature than the latter. This gives rise to more minority-spin electrons in the (5,3) nanotube than in the (6,3) nanotube (see Fig. 4). This also holds for the (4,2) nanotube, which has the same chiral angle as and a larger curvature than the (6,3) nanotube; it exhibits higher occupancies in the minority-spin  $d_{xy}$  and  $d_{zx}$  states and a resulting smaller magnetic moment of  $0.794 \mu_B$ .

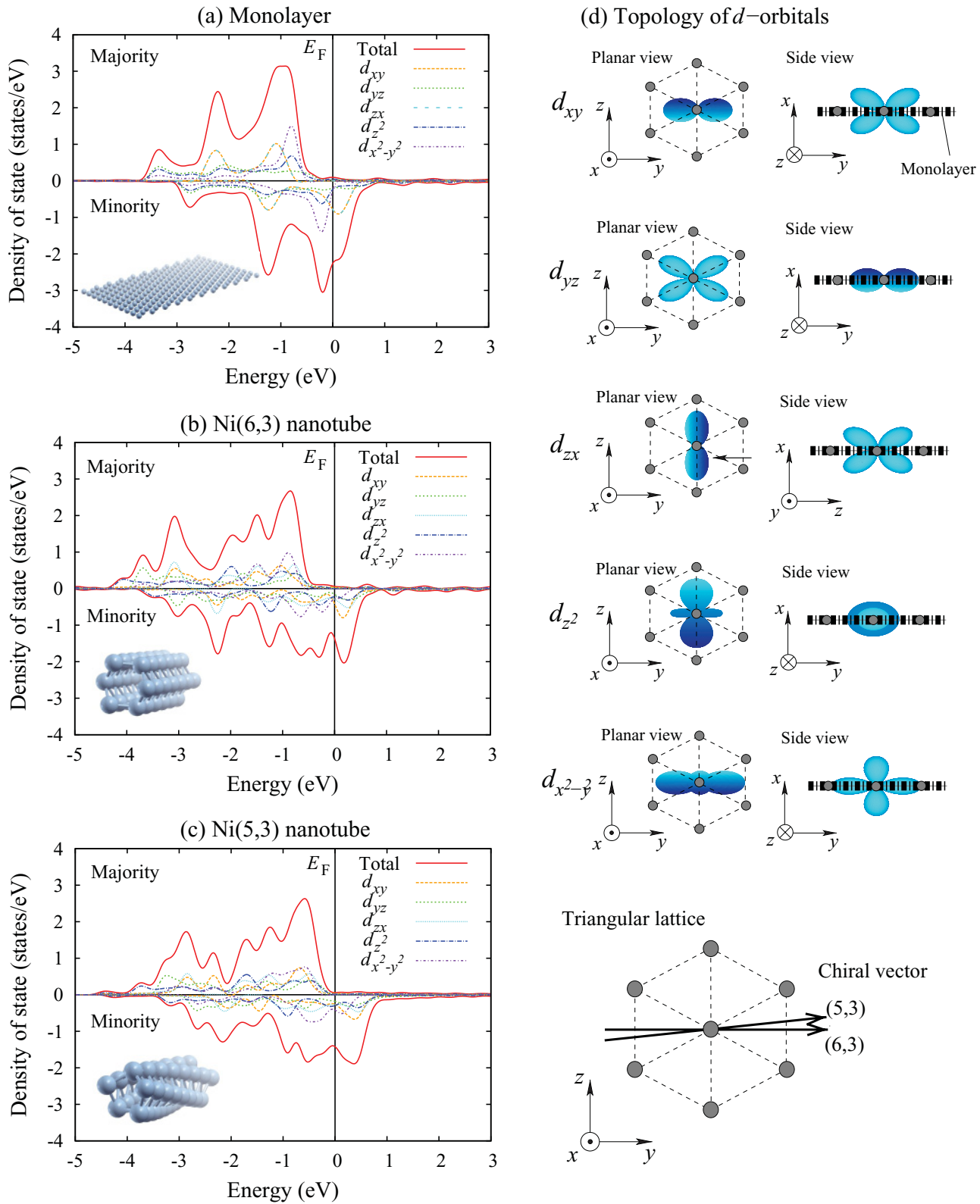


FIG. 5. (Color online) Total and partial  $d$  spin-polarized electronic local density of states (DOS) of the (a) nickel (111) monolayer, and the (b) Ni(6,3) and (c) Ni(5,3) nanotubes. (d) Schematic illustration of topology of  $d$  orbitals on the (111) monolayer. For the nanotubes, the five  $d$  orbitals are taken to be the same direction as those on the monolayer (cf. text).

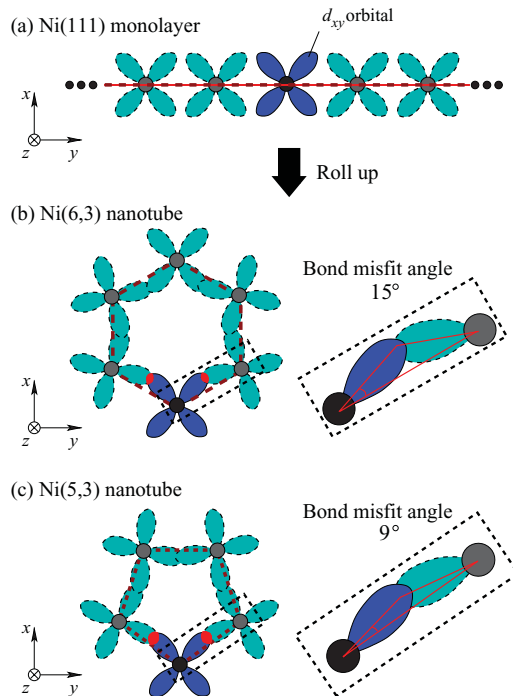


FIG. 6. (Color online) Schematic illustration of the spatial configuration of the  $d_{xy}$  orbital in the (a) nickel monolayer, and the (b) Ni(6,3) and (c) Ni(5,3) nanotubes.

#### IV. CONCLUSION

In this paper, we investigated structural, energetic, electronic, and magnetic properties of ferromagnetic single-wall nickel nanotubes by performing *ab initio* spin-density functional theory calculations. A (6,3) nanotube was found to be energetically favorable as a “magic” structure and it is expected to be observed experimentally in both free-standing and tip-suspended conditions, whereas a (5,3) nanotube is expected to be observed experimentally only for the free-standing case. The (6,3) and (5,3) nanotubes exhibit higher magnetic moments ( $0.864 \mu_B$  and  $0.774 \mu_B$ , respectively) than that of bulk Ni ( $0.635 \mu_B$ ), because they have lower coordination numbers. However, the enhanced magnetic moments of these nanotubes are slightly lower than that of the flat monolayer. This is because the chiral dependence of magnetic moment is predominated by the minority-spin  $d_{xy}$  and  $d_{zx}$  states, in which the out-of-plane  $d$  orbitals interact strongly with each other due to the curvature.

#### ACKNOWLEDGMENTS

This work was supported in part by the Grant-in-Aid for Scientific Research (S) (Grant No. 21226005) and the Grant-in-Aid for Young Scientists (A) (Grant No. 23686023) from the Japan Society of the Promotion of Science (JSPS).

\*shimada@cyber.kues.kyoto-u.ac.jp

- <sup>1</sup>R. T. Senger, S. Dag, and S. Ciraci, *Phys. Rev. Lett.* **93**, 196807 (2004).
- <sup>2</sup>S. L. Elizondo and J. W. Mintmire, *Phys. Rev. B* **73**, 045431 (2006).
- <sup>3</sup>B. Wang, D. Shi, J. Jia, G. Wang, X. Chen, and J. Zhao, *Physica E* **30**, 45 (2005).
- <sup>4</sup>M. Okamoto, T. Uda, and K. Takayanagi, *Phys. Rev. B* **64**, 033303 (2001).
- <sup>5</sup>Y. Kondo and K. Takayanagi, *Science* **289**, 606 (2000).
- <sup>6</sup>Y. Oshima, Y. Kondo, and K. Takayanagi, *J. Electron Microsc.* **52**, 49 (2003).
- <sup>7</sup>Y. Oshima, A. Onga, and K. Takayanagi, *Phys. Rev. Lett.* **91**, 205503 (2003).
- <sup>8</sup>M. Barbic, J. J. Mock, D. R. Smith, and S. Schultz, *J. Appl. Phys.* **91**, 9341 (2002).
- <sup>9</sup>S. Michotte, S. M. Tempfli, and L. Piroux, *Appl. Phys. Lett.* **82**, 4119 (2003).
- <sup>10</sup>T. T. Albrecht, J. Schotter, G. A. Kastle, and N. Emley, *Science* **290**, 2126 (2000).
- <sup>11</sup>E. Tosatti, S. Prestipino, S. Kostlmeier, A. D. Corso, and F. D. D. Tolla, *Science* **291**, 288 (2001).
- <sup>12</sup>X. Yang and J. Dong, *Phys. Rev. B* **71**, 233403 (2005).
- <sup>13</sup>C. K. Yang, *Appl. Phys. Lett.* **85**, 2923 (2004).
- <sup>14</sup>S. P. Ju, J. S. Lin, and W. J. Lee, *Nanotechnology* **15**, 1221 (2004).
- <sup>15</sup>S. P. Ju, W. J. Lee, J. S. Lin, and M. L. Liao, *Mater. Chem. Phys.* **100**, 48 (2006).
- <sup>16</sup>B. Wang, S. Yin, G. Wang, A. Buldum, and J. Zhao, *Phys. Rev. Lett.* **86**, 2046 (2001).

- <sup>17</sup>M. J. Lagos, F. Sato, J. Bettini, V. Rodrigues, D. S. Galvao, and D. Ugarte, *Nature Nanotech.* **4**, 149 (2009).
- <sup>18</sup>S. Konar and B. C. Gupta, *Phys. Rev. B* **78**, 235414 (2008).
- <sup>19</sup>Y. Oshima, H. Koizumi, K. Mouri, H. Hirayama, K. Takayanagi, and A. Kondo, *Phys. Rev. B* **65**, 121401(R) (2002).
- <sup>20</sup>J. Jia, D. Shi, B. Wang, and J. Zhao, *Phys. Rev. B* **74**, 205420 (2006).
- <sup>21</sup>B. Wang, G. Wang, Y. Ren, H. Sun, X. Chen, and J. Zhao, *J. Phys. Condens. Matter* **15**, 2327 (2003).
- <sup>22</sup>B. Wang, G. Wang, and J. Zhao, *Phys. Rev. B* **65**, 235406 (2002).
- <sup>23</sup>B. Wang, G. Wang, and J. Zhao, *Phys. Rev. B* **67**, 193403 (2003).
- <sup>24</sup>O. Gölseren, F. Ercolessi, and E. Tosatti, *Phys. Rev. Lett.* **80**, 3775 (1998).
- <sup>25</sup>M. Zelený, M. Sob, and J. Hafner, *Phys. Rev. B* **79**, 134421 (2009).
- <sup>26</sup>M. Zelený, M. Sob, and J. Hafner, *Phys. Rev. B* **80**, 144414 (2009).
- <sup>27</sup>C. Jo and J. I. Lee, *Phys. Status Solidi B* **241**, 1427 (2004).
- <sup>28</sup>T. Shimada, Y. Ishii, and T. Kitamura, *Phys. Rev. B* **81**, 134420 (2010).
- <sup>29</sup>G. Kresse and J. Hafner, *Phys. Rev. B* **47**, 558 (1993).
- <sup>30</sup>G. Kresse and J. Furthmüller, *Phys. Rev. B* **54**, 11169 (1996).
- <sup>31</sup>P. E. Blöchl, *Phys. Rev. B* **50**, 17953 (1994).
- <sup>32</sup>G. Kresse and D. Joubert, *Phys. Rev. B* **59**, 1758 (1999).
- <sup>33</sup>G. Kresse, W. Bergermayer, and R. Podloucky, *Phys. Rev. B* **66**, 146401 (2002).
- <sup>34</sup>J. P. Perdew, K. Burke, and M. Ernzerhof, *Phys. Rev. Lett.* **77**, 3865 (1996).
- <sup>35</sup>H. J. Monkhorst and J. D. Pack, *Phys. Rev. B* **13**, 5188 (1976).